

Mechanically probing coherent tunnelling in a double quantum dot

J. Gardner¹ and A. A. Clerk¹

¹*Department of Physics, McGill University, Montréal, Québec, Canada H3A 2T8*

(Dated: Sept. 7, 2011)

We study theoretically the interaction between the charge dynamics of a few-electron double quantum dot and a capacitively-coupled AFM cantilever, a setup realized in several recent experiments. We demonstrate that the dot-induced frequency shift and damping of the cantilever can be used as a sensitive probe of coherent inter-dot tunnelling, and that these effects can be used to quantitatively extract both the magnitude of the coherent interdot tunneling and (in some cases) the value of the double-dot T_1 time. We also show how the adiabatic modulation of the double-dot eigenstates by the cantilever motion leads to new effects compared to the single-dot case.

PACS numbers:

Quantum dots have received significant attention both for their applications to quantum information and as laboratories for studies of fundamental physics. Self-assembled, epitaxial quantum dots (QDs) offer advantages over lithographically defined dots in terms of size, confinement potential, and scalability¹. Their small size however makes direct electrical characterization (e.g. via transport) extremely difficult. An alternate approach uses an oscillating atomic force microscope (AFM) tip which is only capacitively coupled to the QD charge^{2–6}. The dot charge acts as a force on the cantilever, and hence its dynamics can alter the cantilever frequency and damping rate. These effects provide detailed information on the dot, similar to that revealed by transport measurements or direct charge-sensing techniques (i.e. using a nearby coupled electrometer). It can even reveal subtle effects involving the interplay between orbital degeneracy and Coulomb blockade physics that are difficult to obtain by other means^{5,7}.

In this work, we focus theoretically on new effects that arise when a low-frequency cantilever is coupled to a double quantum dot (DQD) (i.e. two QDs which are coupled capacitively and via coherent tunnelling^{8,9}). Unlike the single-dot case, the cantilever is now sensitive to variations in the distribution of charge between the two dots. We find that this sensitivity leads to new mechanisms for a dot-induced cantilever damping and frequency shift. These effects are not solely the consequence of incoherent tunnelling to a reservoir (as is the case for a single dot), but instead depend sensitively on the strength of coherent tunnelling between the quantum dots. Our results are derived using a linear-response, quantum master-equation calculation; this extends the semi-classical Fokker-Planck treatments used so often in quantum electromechanics^{5,10–15} to now include coherent interdot tunneling.

The most prominent new effects emerge in the vicinity of the so-called charge transfer line, where two DQD charge configurations having the same total charge are almost degenerate. In this regime, we find a new mechanism for DQD-induced cantilever damping that is enhanced by the relatively long time scale for charge relaxation. We show that this effect can be used to directly measure the T_1 time of the DQD. We also find a new mechanism for a dot-induced cantilever frequency shift near the charge transfer line. In this regime, the presence of coherent tunneling implies that the DQD energy eigenstates are superpositions of charge eigenstates. The oscillator motion can adiabatically modulate the correspond-

ing wavefunctions, which gives rise to the new frequency-shift mechanism. Not surprisingly, as this effect is a direct consequence of having superpositions of charge states, it can be used to probe the strength of coherent interdot tunneling.

Model– Motivated by experiments^{5,7}, we consider a setup where a self-assembled DQD sitting on a surface is capacitively coupled to an oscillating metallic cantilever; the dots are also tunnel-coupled to a two-dimensional electron gas (2DEG) sitting below the surface. The DQD is described by a standard Coulomb blockade Hamiltonian, plus a term describing coherent interdot tunneling (strength $t_c = |t_c|$). We will be interested in the few-electron regime where each dot has at most one electron, and thus retain only a single orbital in each dot; for simplicity, we also treat the case of spinless electrons, as including spin does not significantly change our results.

For a fixed cantilever position, we have:

$$\hat{H}_{\text{DQD}} = \hat{H}_c + t_c \hat{d}_L^\dagger \hat{d}_R + t_c \hat{d}_R^\dagger \hat{d}_L + \hat{H}_{\text{res}} \quad (1)$$

where \hat{d}_α^\dagger is the electron addition operator for dot $\alpha = L, R$. The charging Hamiltonian \hat{H}_c takes the standard form⁸:

$$\hat{H}_c = \sum_{\alpha=L,R} E_{C\alpha} (\hat{n}_\alpha - \mathcal{N}_\alpha)^2 + E_{\text{Cm}} (\hat{n}_L - \mathcal{N}_L) (\hat{n}_R - \mathcal{N}_R). \quad (2)$$

$E_{C\alpha}$ is the charging energy of dot α , E_{Cm} describes their capacitive coupling, and $\hat{n}_\alpha = \hat{d}_\alpha^\dagger \hat{d}_\alpha$ is dot α electron number operator. We focus exclusively on the Coulomb blockade regime where $E_{C\alpha} \gg k_B T$. Finally, \hat{H}_{res} describes the 2DEG as a free electron gas, and dot-2DEG tunneling. We take the 2DEG to be in equilibrium at temperature T , and assume for simplicity that the 2DEG-dot tunnel matrix element is the same for both dots. We use Γ to denote the maximum Golden rule tunnel rate from a given dot to the 2DEG.

The only parameters in \hat{H}_{DQD} depending on the cantilever position \vec{r}_{tip} are the dimensionless gate voltages $\mathcal{N}_\alpha = -V_B C_{\text{tip},\alpha} (|\vec{r}_{\text{tip}} - \vec{r}_\alpha|)/e$, where $C_{\text{tip},\alpha}$ is the cantilever-dot capacitance, \vec{r}_α denotes the position of dot α , and V_B is the voltage applied between the cantilever and the 2DEG. As demonstrated in Refs. 4–6, by varying the tip position at a fixed height above the DQD sample plane, one effectively varies $\mathcal{N}_L, \mathcal{N}_R$ and thus maps out the well-known DQD “stability diagram”⁸ (i.e. realizes different ground-state charge configurations). One can thus effectively view $\mathcal{N}_L, \mathcal{N}_R$ as independent parameters, similar to conventional gated devices.

We now allow the cantilever height z_m to oscillate, letting $z_m = 0$ denote its equilibrium position. The co-ordinate z_m is well-described as a harmonic oscillator having a frequency ω_m and mass m . The coupling between the oscillations and the DQD arises solely through the dependence of the tip-sample capacitance (and hence \mathcal{N}_α) on z_m . For the small oscillations of interest, we can linearize this dependence. Eq. (2) then yields the DQD-cantilever interaction Hamiltonian:

$$\hat{H}_{\text{int}} = -\hat{z}_m \sum_{\alpha=L,R} A_\alpha \hat{n}_\alpha \equiv -\hat{z}_m \hat{F}, \quad (3)$$

$$A_\alpha = 2E_{C\alpha} \frac{\partial \mathcal{N}_\alpha}{\partial z_m} + E_{Cm} \frac{\partial \mathcal{N}_{\bar{\alpha}}}{\partial z_m} = -\frac{\partial E_{+\alpha}}{\partial z_m}, \quad (4)$$

where $\alpha = L, R$ and $\bar{\alpha} = R, L$ are complementary indices. In the last equality, we have introduced the electron addition energies $E_{+\alpha} = E_{C\alpha}(1 - 2\mathcal{N}_\alpha) - E_{Cm}\mathcal{N}_{\bar{\alpha}}$ associated with adding an electron to dot α from the empty DQD state.

We are most interested in the regime where the total DQD charge is fixed at one, and where the electrostatic energy detuning $\delta = (E_{+L} - E_{+R})/2$ of the two relevant charge states $|10\rangle$ (electron on left) and $|01\rangle$ (electron on right) is small. In this regime, we can safely neglect charge states where the total DQD charge is larger than 2. Further, we will focus on DQDs where the coherent tunneling t_c is much larger than both the DQD-2DEG tunneling rate Γ and the mechanical frequency ω_m ; this condition is readily achieved in self-assembled QDs (cf. Ref. 16). It is thus useful to work in the basis of adiabatic eigenstates: the eigenstates of \hat{H}_{DQD} determined by the instantaneous value of z_m . Two of the four eigenstates are simply charge eigenstates: $|1[z_m]\rangle = |11\rangle$, $|4[z_m]\rangle = |00\rangle$. For the remaining eigenstates, note that Eq. (3) implies that the detuning δ will vary linearly with z_m . We thus define:

$$\theta[z_m] = \arctan \left[\frac{t_c}{\delta[z_m]} \right] = \arctan \left[\frac{t_c}{\delta - z_m(A_L - A_R)/2} \right]. \quad (5)$$

The remaining adiabatic eigenstates are thus:

$$|2[z_m]\rangle \equiv |g[z_m]\rangle = -\sin(\theta/2) |10\rangle + \cos(\theta/2) |01\rangle \quad (6a)$$

$$|3[z_m]\rangle \equiv |e[z_m]\rangle = \cos(\theta/2) |10\rangle + \sin(\theta/2) |01\rangle, \quad (6b)$$

with corresponding adiabatic eigenenergies

$$E_{g,e}[z_m] = \left(\frac{E_{+L} + E_{+R} - (A_L + A_R)z_m}{2} \right) \mp \sqrt{[\delta[z_m]]^2 + t_c^2} \\ \equiv \bar{\epsilon}[z_m] \mp \Delta[z_m]. \quad (7)$$

For $z_m = 0$, the DQD will primarily occupy the states $|2\rangle \equiv |2[0]\rangle$ and $|3\rangle \equiv |3[0]\rangle$, and thus will approximate the physics of a two-level system..

Calculation— As a result of the coupling in Eq. (3), the average force from the dot $\langle \hat{F} \rangle$ will respond with a delay to the motion of the oscillator resulting in both a spring-constant shift k_{dot} and extra damping γ_{dot} ; for the weak couplings of interest, this is fully described within linear response¹⁷. To quantitatively describe these effects in the regime $\hbar\omega_m \ll k_B T$, we derive a Lindblad master equation describing the DQD and cantilever. For a single-QD system, this approach

yields a classical master equation with incoherent tunnelling rates set by the instantaneous oscillator position^{5,10–15}. To extend this approach to include coherent tunneling, note that since we will calculate k_{dot} and γ_{dot} within linear response, we can without loss of generality replace the cantilever position \hat{z}_m by its average value: $\hat{z}_m \rightarrow z_m(t) = z_0 \cos(\omega_m t)$. Understanding how the DQD responds to this time-dependent classical field will then yield k_{dot} and γ_{dot} . Defining $\hat{U}[x]$ via $\hat{U}[x]|j[0]\rangle = |j[x]\rangle$, we define $\hat{\rho}_{\text{rot}}(t) = \hat{U}[z_m(t)]^\dagger \hat{\rho}(t) \hat{U}[z_m(t)]$, where $\hat{\rho}(t)$ is the Schrödinger-picture reduced density matrix of the DQD. $\hat{\rho}_{\text{rot}}$ is simply the DQD density matrix in the adiabatic basis. Using the experimentally-relevant conditions $|t_c| \gg \hbar\Gamma$ and $(\bar{A}_{L,R} z_0 \hbar\omega_m) \ll (k_B T)^2$, and making Born-Markov and secular approximations, we obtain:

$$\frac{\partial \hat{\rho}_{\text{rot}}}{\partial t} = \frac{1}{i\hbar} [\hat{H}_{\text{eff}}, \hat{\rho}_{\text{rot}}] + \sum_{j,k=1}^4 \Gamma_{jk} \mathcal{D}[\hat{S}_{jk}] \hat{\rho}_{\text{rot}}. \quad (8)$$

The first term on the RHS describes coherent evolution. Using Pauli matrices to describe the states $|2\rangle, |3\rangle$ as a two-level system in the natural way, e.g. $\hat{\sigma}_z = |3\rangle\langle 3| - |2\rangle\langle 2|$, $\hat{\sigma}_x = |3\rangle\langle 2| + |2\rangle\langle 3|$, $\hat{\sigma}_y = i(|2\rangle\langle 3| - |3\rangle\langle 2|)$, we find:

$$\hat{H}_{\text{eff}} = \bar{\epsilon} \hat{n}_{\text{tot}} + E_m |4\rangle\langle 4| + \Delta \hat{\sigma}_z - \frac{\hbar}{2} \frac{\partial z_m}{\partial t} \frac{\partial \theta}{\partial z_m} \hat{\sigma}_y, \quad (9)$$

The last term here describes an effective state precession; its origin is the rotation of the adiabatic eigenstates brought on by $z_m(t)$. Note that similar adiabatic approaches have been used to study periodically-modulated, dissipative two-level systems, with the dissipation being treated phenomenologically^{18–22}, or as a bosonic bath²³. In contrast, our system is effectively a four state system, and the dominant dissipation due to 2DEG tunneling is treated microscopically.

The remaining terms on the RHS of Eq. (8) have the standard form of Lindblad dissipation. Letting $\hat{S}_{jk} = |j\rangle\langle k|$, the superoperators $\mathcal{D}[\hat{S}_{jk}]$ are defined as:

$$\mathcal{D}[\hat{S}_{jk}] \hat{\rho}_{\text{rot}} = \hat{S}_{jk} \hat{\rho}_{\text{rot}} \hat{S}_{jk}^\dagger - \frac{1}{2} (\hat{S}_{jk}^\dagger \hat{S}_{jk} \hat{\rho}_{\text{rot}} + \hat{\rho}_{\text{rot}} \hat{S}_{jk}^\dagger \hat{S}_{jk}), \quad (10)$$

In the case where the total charge in states $|j\rangle$ and $|k\rangle$ differ by 1, Γ_{jk} is simply a Fermi Golden rule rate for DQD-2DEG tunneling determined by the *instantaneous* eigenstate energies $E_j[z_m(t)]$, $E_k[z_m(t)]$. In contrast, the rates Γ_{23}, Γ_{32} describe the intrinsic relaxation of the DQD, with $1/T_{1,\text{int}} \equiv \Gamma_{23} + \Gamma_{32}$. We will treat such processes phenomenologically by taking $1/T_{1,\text{int}}$ to be a parameter. We also assume that the bath responsible for the intrinsic relaxation has the same temperature as the 2DEG; as such, the $z_m = 0$ stationary solution of Eq. (8) is simply a thermal occupation of the states $|j\rangle$. To find the dot-induced damping and spring-constant shift of the cantilever, we use Eq. (8) to find the first-order-in- z correction to $\hat{\rho}_{\text{rot}}$, and use the corresponding change in $\langle \hat{F}(t) \rangle$ to get γ_{dot} and k_{dot} in the standard manner (see, e.g., Ref.¹⁷).

Basic mechanisms— In the low-frequency limit, the linear-response results take the form:

$$m\gamma_{\text{dot}} = \tau \frac{\partial \langle \hat{F} \rangle}{\partial z_m}, \quad k_{\text{dot}} = -\frac{\partial \langle \hat{F} \rangle}{\partial z_m} \quad (11)$$

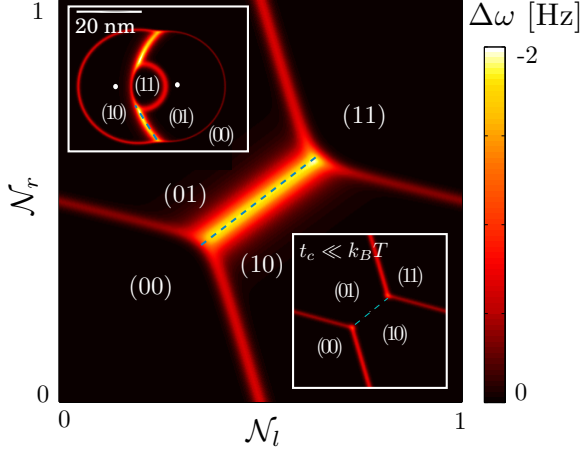


FIG. 1: Calculated DQD-induced frequency shift $\Delta\omega = k_{\text{dot}}/(2m\omega_m)$, using parameter values similar to the experiment of Ref.⁵. Main plot: frequency shift versus dimensionless gate voltage for $\omega_m = 160$ kHz, $k_0 = 7$ N/m, $\Gamma = 10$ kHz, $T = 4.2$ K, $t_c = 1$ meV, $E_{CL} = 20$ meV, $E_{CR} = 25$ meV, $E_{Cm} = 12$ meV. Most interesting is the feature along the charge transfer line (indicated with a dashed line), which results from the adiabatic modulation of the DQD eigenstates by the cantilever. The width of this feature is a measure of t_c . For simplicity, we have used fixed couplings $A_L \approx 8$ meV/nm, $A_R \approx 6$ meV/nm. Lower inset: Same as main plot, but now $t_c = 0.001$ meV $\ll k_B T$. The adiabatic feature is absent. Upper inset: Simulated AFM data of frequency-shift versus lateral tip position, for a tip height of 20 nm and a bias voltage $V_B = -7.1$ V; white dots indicate the centres of the two dots. The parameters and coherent tunneling are the same as the main plot, but the couplings A_L, A_R now vary with tip position. See Supplemental Material for more details²⁵.

where τ is an effective response time¹⁷. In the single dot case, the static susceptibility $\partial\langle\hat{F}\rangle/\partial z_m$ is just proportional to the charge susceptibility $\partial\langle\hat{n}_{\text{tot}}\rangle/\partial\mathcal{N}$. γ_{dot} and k_{dot} are thus only significant when the QD is tuned to a point where its total charge can fluctuate via 2DEG-QD tunneling; correspondingly, $\tau \sim 1/\Gamma$. In contrast, these fluctuations of total charge are exponentially suppressed in a DQD near the charge transfer line. As we now show, γ_{dot} and k_{dot} are instead determined by the response and dynamics of the DQD charge distribution.

In the vicinity of the charge transfer line, the DQD-induced force operator \hat{F} takes the form ($A_\delta = (A_L - A_R)/2$):

$$\hat{F} - \frac{A_L + A_R}{2} \simeq A_\delta (\hat{n}_L - \hat{n}_R) = A_\delta (\cos\theta \hat{\sigma}_z - \sin\theta \hat{\sigma}_x) \quad (12)$$

It follows that both γ_{dot} and k_{dot} will have contributions from three distinct mechanisms, corresponding to the susceptibilities $\partial_{z_m}\langle\hat{\sigma}_x\rangle$, $\partial_{z_m}\langle\hat{\sigma}_z\rangle$ and $\partial_{z_m}\theta$. The first of these involves the oscillator motion modifying the coherence between the $|e\rangle$ and $|g\rangle$ DQD eigenstates. This corresponds to the well-known resonant-damping mechanism of acoustic vibrations by a two-level system^{19,20,24}, and is strongly suppressed in our system as $\hbar\omega_m \ll t_c$; we thus do not discuss it further. The remaining two mechanisms are important for our system, and we discuss their effects in turn.

Adiabatic frequency shift– Eq. (12) implies that as \hat{F} has an explicit dependence on θ , the intrinsic z_m -dependence of θ (cf. Eq. (5)) will cause a modulation of \hat{F} . Physically, this corresponds to the adiabatic modulation of the DQD eigenstates by the cantilever oscillation (via the the cantilever’s modulation of the electrostatic detuning δ). The corresponding oscillation in $\langle\hat{n}_L - \hat{n}_R\rangle$ causes a force oscillation which is in phase with $z_m(t)$; it thus contributes a to the DQD-induced spring-constant shift k_{dot} . One finds simply:

$$k_{\text{dot,ad}} = -A_\delta \langle\hat{\sigma}_z\rangle \frac{\partial \cos\theta}{\partial z_m} = \frac{-A_\delta^2 \sin^2\theta \tanh(\Delta/k_B T)}{\Delta} \quad (13)$$

where the RHS should be evaluated at $z_m = 0$. Note that as we focus on a small cantilever frequency ($\hbar\omega_m \ll t_c^2/(z_0 A_\delta)$), non-adiabatic Landau-Zener transitions will have negligible probability and can be safely neglected. Such non-adiabatic transitions were recently studied in a two-mode optomechanical system²⁶; unlike our work, the focus was on the regime where ω_m was much larger than the effective tunneling t_c . We stress that $k_{\text{dot,ad}}$ is a direct consequence of having coherent interdot tunneling, and vanishes in the limit $t_c \rightarrow 0$. It is most pronounced at low temperatures ($k_B T < t_c$), where it gives rise to a feature near the charge transfer line whose width (in δ) is $\sim t_c$. Further, at such low temperatures this effect dominates all other contributions to k_{dot} near the charge transfer line. The effect thus provides a direct means for both detecting the presence of coherent interdot tunneling, and for measuring its magnitude.

Shown in Figure 1 is a full calculation of the DQD-induced frequency shift $\Delta\omega = k_{\text{dot}}/(2m\omega_m)$ obtained using Eq. (8) and linear response, keeping all contributions. We have used experimentally-relevant DQD and cantilever parameters; see caption for details. The lower inset shows results for a small value of t_c ; similar to a single QD system, the only appreciable frequency shift occurs at charge addition lines where lead tunneling is strong and the total dot charge can fluctuate. In contrast, for a larger value of t_c , one obtains a large frequency shift along the charge transfer line, in agreement with Eq. (13). Again, seeing this effect provides a direct probe of coherent interdot tunneling. Note that there exists a somewhat similar adiabatic contribution to the TLS - acoustic wave interaction in glasses²¹, but that it is neglected in the standard early treatments^{18–20}.

Effective TLS damping– Eq. (12) indicates a second mechanism which contributes to k_{dot} and γ_{dot} near the charge transfer line: the cantilever’s modulation of $\langle\sigma_z\rangle$, the population asymmetry of the two low-energy DQD eigenstates. This corresponds directly to the well-known mechanism of non-resonant damping by a two-level system (TLS), studied both in the context of acoustic damping in glasses^{18–23,27}. On a heuristic level, the cantilever oscillations cause the DQD splitting Δ to oscillate (cf. Eq. (7)), which in turn causes the occupancy of the states $|2\rangle, |3\rangle$ to oscillate. The corresponding oscillations in $\langle\hat{\sigma}_z\rangle$ (and hence $\langle\hat{F}\rangle$) are phase shifted with respect to $z_m(t)$ due to the finite DQD T_1 time; the mechanism thus contributes both to γ_{dot} and k_{dot} . Note that this mechanism is suppressed at low temperatures $k_B T \ll \Delta$, as in this case the DQD is always in its ground state.

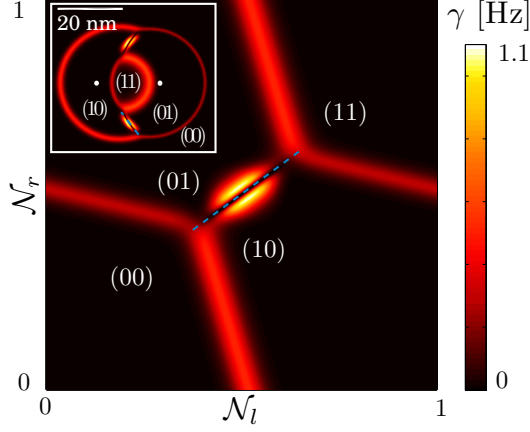


FIG. 2: Calculated DQD-induced damping γ_{dot} . DQD parameters are identical to Figure 1, except for $t_c = 0.3$ meV, $T = 8.4$ K, and $\Gamma = 10$ MHz. We have also included an intrinsic relaxation mechanism ($T_{1,\text{int}}^{-1} \sim 100$ kHz) which imposes a lower bound on the TLS relaxation rate. The AFM tip parameters are $\omega_m = 75$ kHz and $k_0 = 3$ N/m. The main plot shows the damping as a function of the dimensionless gate voltages, while the inset shows a simulated AFM damping-versus-position image. The damping features near the charge transfer line correspond to the TLS damping mechanism discussed in the text.

We find that the DQD-induced damping due to this mechanism is given by:

$$m\gamma_{\text{dot}} = \left(\frac{T_1}{1 + \omega_m^2 T_1^2} \right) \frac{A_\delta^2 \cos^2 \theta}{k_B T \cosh^2(\Delta/k_B T)}, \quad (14)$$

in agreement with previous works. Unlike previous works, we know what the TLS here is (i.e. the DQD), and also know at least some of the processes contributing to its relaxation time T_1 . For our model of spinless electrons, we find:

$$T_1^{-1} = \Gamma \cosh(\beta \Delta) (e^{-\beta |\epsilon|} + e^{\beta (|\epsilon| - E_m)}) + T_{1,\text{int}}^{-1}, \quad (15)$$

where $\beta = 1/(k_B T)$. The first term corresponds to relaxation processes involving 2DEG-DQD tunneling and an intermediate state where the total DQD charge is either 2 or 0; the second term corresponds to intrinsic relaxation processes. The spin-full case is given in the Supplemental Material²⁵.

One might naïvely think that significant dot-induced damping could only occur near charge addition lines where DQD-2DEG tunneling is strong. However, for a low frequency cantilever, we see that near the charge transfer line, γ_{dot} scales as

T_1 ; in contrast, the more conventional γ_{dot} mechanism near a charge addition line scales as $1/\Gamma$. Thus, if $T_1 \Gamma > 1$, this “TLS damping” mechanism can be equal to or even greater in magnitude than the more conventional damping peaks found near charge addition lines. This behaviour is shown in Figure 2, where we use our full calculation to plot the DQD contribution to the cantilever damping, γ_{dot} . It is interesting to note the presence of coherent tunneling causes the effect to vanish at $\delta = 0$, as Δ has no linear dependence on z_m here. One can thus use the suppression of this damping effect on the charge transfer line as a direct probe of coherent interdot tunneling.

Measuring T_1 — In the simple case of a low frequency cantilever and a single mechanism contributing to both k_{dot} and γ_{dot} , Eq. (11) suggests that one can simply measure the relevant response time τ by taking the ratio of the two effects, without having to precisely know the strength of the dot-cantilever coupling. A similar approach can be used to extract the DQD T_1 time near the charge transfer line, though more care is needed, as there are two mechanisms contributing to k_{dot} . First, note that the γ_{dot} as given by Eq. (14) is only appreciable for $k_B T \gtrsim \Delta$. For $k_B T \gg \Delta$, one finds that the two spring constant mechanisms combine in a particularly simple manner, and that the damping versus spring constant shift ratio takes the simple form:

$$\frac{m\gamma_{\text{dot}}}{k_{\text{dot}}} \simeq -\cos^2 \theta T_1. \quad (16)$$

By fitting the experimentally-measured γ_{dot} and k_{dot} to this formula near the charge transfer line, one can thus get a direct measure of the DQD T_1 time. This shows an advantage of this technique over conventional charge-sensing: as one is measuring dynamic phenomena (as opposed to simply the average value of the charge in the two dots), it is possible to directly extract important DQD timescales.

Conclusions— Using a somewhat novel master equation approach in conjunction with linear response, we have studied theoretically how charge dynamics in a DQD can cause damping and frequency shifts of a low-frequency mechanical resonator (such as an AFM tip). Qualitatively new effects arise compared to the case of a single dot due to the cantilever’s sensitivity to charge distribution, and due to the presence of coherent interdot tunneling. We demonstrated that these effects could be used to detect and measure the magnitude of coherent tunneling, as well as extract the DQD T_1 time near the charge transfer line.

The authors acknowledge research support from CIFAR, NSERC and the McGill Centre for the Physics of Materials.

¹ H. Drexler et al., Phys. Rev. Lett. **73**, 2252 (1994).

² M. Woodside and P. L. McEuen, Science **296**, 1098 (2002).

³ J. Zhu, M. Brink, and P. L. McEuen, Appl. Phys. Lett. **87**, 242102 (2005).

⁴ R. Stomp et al., Phys. Rev. Lett. **94**, 056802 (2005).

⁵ L. Cockins et al., Proc. Nat. Acad. Sci. **107**, 9496 (2010).

⁶ A. Dăna and Y. Yamamoto, Nanotechnology **16**, S125 (2005).

⁷ S. D. Bennett et al., Phys. Rev. Lett. **104**, 017203 (2010).

⁸ W. G. van der Wiel et al., Rev. Mod. Phys. **75**, 1 (2002).

⁹ L. Wang et al., Adv. Mater. **21**, 2601 (2009).

- ¹⁰ A. D. Armour, M. P. Blencowe, and Y. Zhang, Phys. Rev. B **69**, 125313 (2004).
- ¹¹ N. M. Chtchelkatchev, W. Belzig, and C. Bruder, Phys. Rev. B **70**, 193305 (2004).
- ¹² Y. M. Blanter, O. Usmani, and Y. V. Nazarov, Phys. Rev. Lett. **93**, 136802 (2004).
- ¹³ F. Pistolesi and S. Labarthe, Phys. Rev. B **76**, 165317 (2007).
- ¹⁴ D. A. Rodrigues and A. D. Armour, New J. Phys. **7**, 251 (2005).
- ¹⁵ C. B. Doiron, W. Belzig, and C. Bruder, Phys. Rev. B **74**, 205336 (2006).
- ¹⁶ S. Amaha et al., Appl. Phys. Lett. **92**, 202109 (2008).
- ¹⁷ A. A. Clerk and S. D. Bennett, New J. Phys. **7**, 238 (2005).
- ¹⁸ J. Jäckle et al., J. Non-Cryst. Solids **20**, 365 (1976).
- ¹⁹ B. Golding et al., Phys. Rev. Lett. **30**, 223 (1973).
- ²⁰ S. Hunklinger and W. Arnold, *Ultrasonic Properties of Glasses at Low Temperatures*, vol. XII (Academic Press, New York, New York, 1976).
- ²¹ J. T. Stockburger, M. Grifoni, and M. Sassetti, Phys. Rev. B **51**, 2835 (1995).
- ²² D. A. Parshin, Z. Phys. B **91**, 367 (1993).
- ²³ M. Grifoni and P. Hänggi, Phys. Rep. **304**, 229 (1998).
- ²⁴ L. G. Remus, M. P. Blencowe, and Y. Tanaka, Phys. Rev. B **80**, 174103 (2009).
- ²⁵ See supplementary material at XXX for further details.
- ²⁶ G. Heinrich, J. G. E. Harris, and F. Marquardt, Phys. Rev. A **81**, 011801 (2010).
- ²⁷ A. N. Cleland, *Foundations of Nanomechanics* (Springer, New York, New York, 2003).